Shear Stress from Rate-Dependent and Nonaffine Network Models for Melts in Complex Shear Histories

Y. Z. XU, C. F. CHAN MAN FONG, and D. DE KEE*

Department of Chemical Engineering, University of Sherbrooke, Sherbrooke, Quebec J1K 2R1, Canada

SYNOPSIS

Analytical expressions of shear stress for arbitrary multi-rate-step flows are presented for a rate-dependent network model and for a nonaffine network model. For both models the linear spectrum is modified to account for large deformations. Predictions of both models are evaluated for the following cases: concave steps, reversed steps, and large amplitude oscillations. Model predictions are compared to experimental results on a polydimethylsiloxane melt. Quantitative agreement is obtained for both models, which justifies the usefulness of the proposed equations for the prediction of shear responses in complex transient shear flows. The performance and limitations of the two models are also discussed in terms of physical considerations. © 1996 John Wiley & Sons, Inc.

INTRODUCTION

Industrial processes involving the flow of polymer melts, solutions, and suspensions are associated with complex time-dependent flow histories. To model these flows successfully we need constitutive equations that can describe the main rheological properties of the materials. Transient flows, and in particular multistep flows, provide severe tests for the evaluation of constitutive equations.[1]

Several such tests have been performed and the general consensus is that so far no equation can adequately describe polymeric materials in very complex flow situations.[2-6]

In a previous article we compared the experimental data on polyethylene in shear-rate reduction and interrupted shear flows with the predictions of a rate-dependent network (RDN) model and a nonaffine network (NAN) model.[7] In this article we further explore the capabilities of these two models by considering a concave step, a reverse step, and large amplitude oscillatory flow. The predictions are compared with experimental data on a polydimethylsiloxane (PDMS) melt.

* To whom correspondence should be addressed.

Journal of Applied Polymer Science, Vol. 59, 1099-1105 (1996)
 CCC 0021-8995/96/071099-07

THEORY

The constitutive equation of an RDN model, using the memory function proposed by De Kee, can be written as[8]

$$\tau = -p\mathbf{I} + \int_{-\infty}^{t} m[t-t', \Pi(t,t')]\mathbf{G}(t,t')\,dt' \quad (1a)$$

$$m[t-t', \Pi(t,t')] = \sum_{p=1}^{m} \frac{\eta_p f_p[\Pi(t')]}{\lambda_p^2} \exp\left[-\int_{t'}^{t} \frac{dt''}{\lambda_p g_p[\Pi(t'')]}\right] \quad (1b)$$

$$f_p = f_0 \exp\{-(|\Pi|/2)^{1/2}(-2c+3)t_p\} \quad (1c)$$

$$g_p = \exp\{-(|\Pi|/2)^{1/2}(c-1)t_p\} \quad (1d)$$

where τ is the stress tensor; p, the isotropic pressure; I, the unit tensor; $\mathbf{G}$, the reduced relative Finger tensor; η_p, λ_p, and t_p are constants associated with the pth relaxation mode; c and f_0 are constants; and Π is the second invariant of the shear rate.

In an arbitrary multi-rate-step flow history as shown in Figure 1, a constant shear rate $\dot{\gamma}_k$ is maintained between times t_{k-1} and t_k. The shear stress τ_{21} at the present time t $(=t_n)$, can be written as[7]

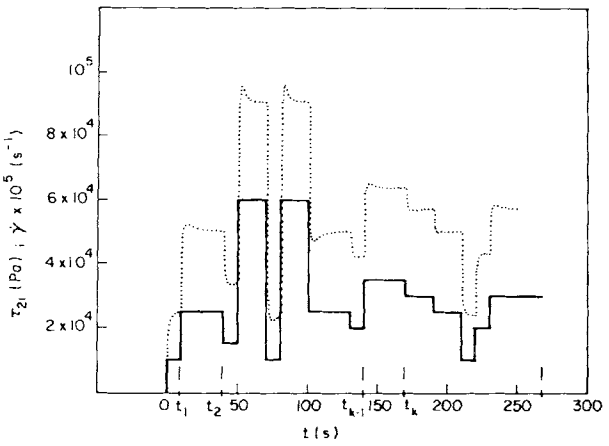

Figure 1 A schematic view of an arbitrary multi-rate-step flow. (· · ·) Calculated stress curve is based on an RDN model for PDMS data. (—) $\dot{\gamma}$.

$$\tau_{21}(t) = \sum_{k=0}^{n} I_k \tag{2a}$$

$$I_k = \sum_{p=1}^{m} \frac{\eta_p f_{p,k}}{\lambda_p} \exp\left[\sum_{i=k}^{n-1} \frac{t_i}{\lambda_p}\left(\frac{1}{g_{p,i+1}} - \frac{1}{g_{p,i}}\right)\right] \times \left\{g_{p,k}\left[\sum_{i=k}^{n-1} t_i(\dot{\gamma}_i - \dot{\gamma}_{i+1}) + \dot{\gamma}_n t_n\right](e^{t_k/\lambda_p g_{p,k}} - e^{t_{k-1}/\lambda_p g_{p,k}}) - \dot{\gamma}_k g_{p,k}[(t_k - \lambda_p g_{p,k})e^{t_k/\lambda_p g_{p,k}} - (t_{k-1} - \lambda_p g_{p,k})e^{t_{k-1}/\lambda_p g_{p,k}}]\right\} e^{-t/\lambda_p g_{p,n}}. \tag{2b}$$

The constitutive equation of the chosen NAN model is written as

$$\tau = -p\mathbf{I} + \int_{-\infty}^{t} G(t-t')\mathbf{E}(t,t')\mathbf{D}^*(t') \times \mathbf{E}^{\dagger}(t,t')\,dt' \tag{3a}$$

$$\frac{\partial \mathbf{E}(t,t')}{\partial t} = \mathbf{A}(t)\mathbf{E}(t,t'), \quad \mathbf{E}(t',t') = \mathbf{I} \tag{3b, c}$$

$$G(t-t') = \sum_{p=1}^{m} G_p e^{-(t-t')/\lambda_p} \tag{3d}$$

$$\mathbf{D}^* = \tfrac{1}{2}(\mathbf{A} + \mathbf{A}^{\dagger}) = a(\Pi)\mathbf{D} \tag{3e}$$

where $\mathbf{D}$ is the rate of deformation tensor; $a(\Pi)$, a slip factor; and $\mathbf{A}$, the velocity gradient in the slip frame.

The shear stress $\tau_{21}(t)$ at time t ($=t_n$) in a multi-rate-step flow history is given by[7]

$$\tau_{21} = \sum_{k=1}^{n} S_k \tag{4a}$$

$$S_k = \frac{a_k \dot{\gamma}_k}{2} \sum_{p=1}^{m} \frac{G_p e^{-(t/\lambda_p)}}{\lambda_p^{-2} + \beta_k^2} \times [e^{t_k/\lambda_p}\{\lambda_p^{-1}\cos(\alpha_k - \beta_k t_k) - \beta_k \sin(\alpha_k - \beta_k t_k)\} - e^{t_{k-1}/\lambda_p}\{\lambda_p^{-1}\cos(\alpha_k - \beta_k t_{k-1}) - \beta_k \sin(\alpha_k - \beta_k t_{k-1})\}] \tag{4b}$$

where

$$\alpha_k = 2\xi_k\left\{\sum_{i=k+1}^{n} \dot{\gamma}_i(t_i - t_{i-1}) + \dot{\gamma}_k t_k\right\} \tag{4c}$$

$$\beta_k = 2\xi_k \dot{\gamma}_k \tag{4d}$$

$$\xi_k = \sqrt{1 - a_k^2}. \tag{4e}$$

EXPERIMENTAL

The polymer melt sample chosen is PDMS, a viscoelastic standard material provided by the Rheometrics Co. All rheological measurements were performed at 298 K using a Rheometrics RMS-800 cone and plate rheometer with a cone angle of 0.1 rad and a diameter of 25 mm.

The data for the dynamic moduli G' and G'' versus frequency ω are plotted in Figure 2. The linear relaxation time spectrum is calculated via Tschoegl's second approximation[9,10]:

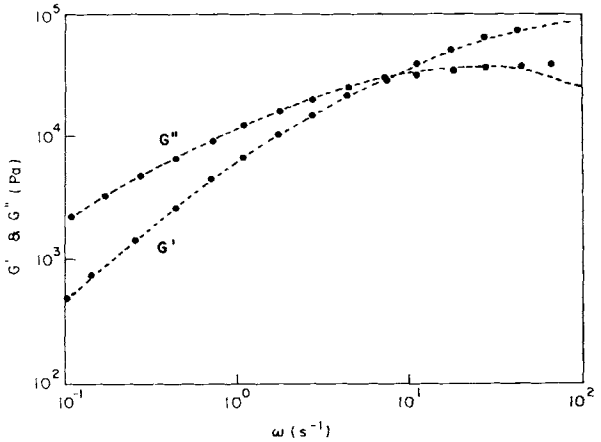

Figure 2 The dynamic moduli G' and G'' as functions of frequency. (●) Data and (- - -) calculated curves from the discrete relaxation time spectrum in Table I for the PDMS sample.

$$H(\lambda) = \left[\frac{dG'}{d \ln \omega} - \frac{1}{2}\frac{d^2G'}{d(\ln \omega)^2}\right]_{1/\omega=\lambda/\sqrt{2}}. \quad (5)$$

A set of discrete values for the relaxation times λ_p and moduli G_p are selected from the continuous spectrum according to the following equations

$$G_p = H_p \Delta \ln \lambda_p \quad (6a)$$

$$\eta_p = G_p \lambda_p. \quad (6b)$$

The values of the discrete spectrum for both models are shown in Table I.

As a check of the procedure used to obtain the spectra, the values were used to calculate G' and G'' from the generalized Maxwell model:

$$G' = \sum_{p=1}^{m} \frac{G_p \lambda_p^2 \omega^2}{1 + (\lambda_p \omega)^2} \quad (7a)$$

$$G'' = \sum_{p=1}^{m} \frac{G_p \lambda_p \omega}{1 + (\lambda_p \omega)^2} \quad (7b)$$

and the results are shown as broken lines in Figure 2.

The steady shear viscosity and the dynamic viscosity data are plotted in Figure 3. The values of the viscosity at high shear rates are the absolute values of the complex viscosity, assuming the Cox–Merz rule to be valid.

The material parameters in the RDN model are λ_p, η_p, f_0, and c. The number of modes and hence the number of parameters can be chosen to fit the data. Using the data obtained from the dynamic tests, under the assumptions that $\eta_p = G_p\lambda_p$, all the parameters are fixed except for c. In the linear region, f_p is unity. In the nonlinear regime, f_0 is not equal to one. It can be considered as an adjustable parameter to fit the data when the deformation can no longer be considered to be small. In the case of the NAN model, the only adjustable parameter is a. It will be seen later that the values of G_p deduced from the dynamic data are too low to fit the experimental data for large deformations.

Table I Discrete Relaxation Time Spectrum for PDMS at 298 K

	Spectrum	
Relaxation Time, λ_p (s)	NAN G_p (Pa)	RDN η_p (Pa s)
0.01000	3154.4	31.54
0.02187	35310.6	772.25
0.04782	24613.3	1176.5
0.10456	17151.6	1793.4
0.22865	11051.5	2527.0
0.50000	6412.8	3026.4
1.09336	3295.5	3601.4
2.39088	1518.4	3629.0
5.22820	650.9	3402.9
11.4326	260.2	2974.1
25.0000	0.004	0.1

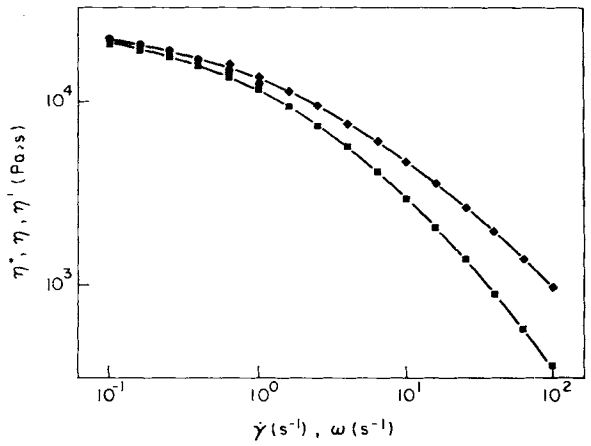

Figure 3 (■) The dynamic viscosity η' and the complex viscosity η^* as functions of frequency ω together with (●) the steady shear viscosity η as a function of shear rate $\dot{\gamma}$ for the PDMS sample. (♦) Calculated values assuming the Cox–Merz rule to be valid.

DISCUSSION

We compare the theoretical predictions with the experimental observations for the following flows.

Concave-Rate Step Flows

In a concave-rate step flow, a constant shear rate is maintained and is then decreased. The flow is kept at the lower shear rate for a length of time. Unlike the strain-rate reduction experiment, in this case the strain rate is increased to the initial shear rate, and after a lapse of time the flow is stopped. This is shown in Figure 4. The corresponding shear stress for the RDN model can be calculated from eq. (2a, b). Figure 4 shows the shear stress for one set of values of λ_p, η_p and for various values of the adjustable parameter c. We note that the lower the values of c, the higher the overshoot and the lower the undershoot. The values of c do not affect the steady values of the shear stress and the stress relaxation.

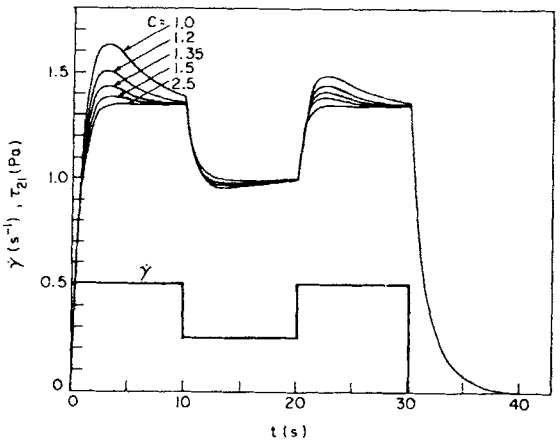

Figure 4 Transient behavior of shear stress for a RDN fluid for different values of the parameter c in a concave step flow ($\dot{\gamma}$ = 0.5, 0.25, 0.5, 0.0 s^{-1}). Model parameters are: $\lambda_1 = 1$, $\lambda_2 = 2$, $\eta_1 = 2$, and $\eta_2 = 4$.

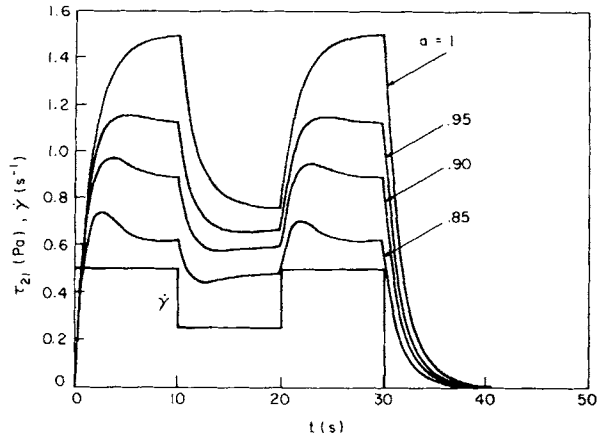

Figure 6 Variation of the shear stress of a NAN fluid. Effect of the slip parameter a in a concave step flow ($\dot{\gamma}$ = 0.5, 0.25, 0.5, 0.0 s^{-1}). The model parameters are $\lambda_1 = 1$, $\lambda_2 = 2$, $G_1 = G_2 = 2$.

The second overshoot is found to be lower than the first one. This is due to the preshearing of the material.

Figure 5 compares the predictions of the RDN model with the PDMS data for several step rates. It can be seen that there is reasonably good agreement for both transient and steady values of the stress. The model predicts a higher overshoot that occurs earlier than the one obtained experimentally. Adding more modes to the calculation of the stress does not appreciably improve the overshoot predictions.

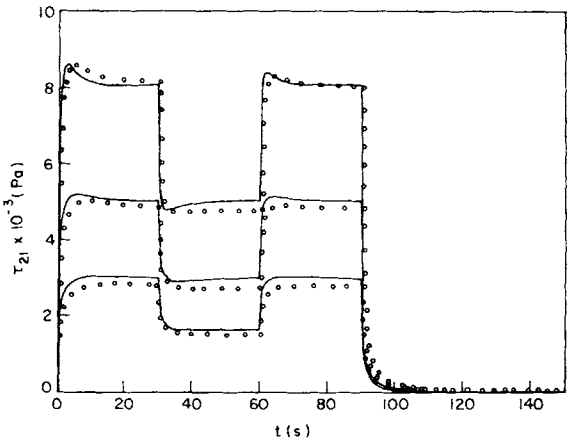

Figure 5 Comparison of (O) the measured shear stress with the RDN model predictions for concave steps with different levels: (1) upper curve: $\dot{\gamma}$ = 0.5, 0.25, 0.5, 0.0 s^{-1}; (2) $\dot{\gamma}$ = 0.25, 0.125, 0.25, 0.0 s^{-1}; (3) lower curve: $\dot{\gamma}$ = 0.125, 0.06, 0.125, 0.0 s^{-1}. The calculation is based on the measured spectrum from dynamic data for a PDMS sample and with $c = 1.3$ and $f_0 = 1.45$ for all steps.

The shear stress for the NAN model can be calculated from eq. (4a–e) and is shown in Figure 6 for one set of values of λ_p, G_p and various values of the adjustable parameter a. The lower the values of a, the lower the predicted values of the shear stress. We note the absence of a stress overshoot in the case where $a = 1$. Stress overshoot occurs only for values of $a < 1$. This implies that for the NAN model, slippage must be present for stress overshoot to occur. The lower the value of a, the faster the stress will decay to zero when the flow has stopped.

Figure 7 shows a comparison of the predicted values of the NAN model with the experimental values of the PDMS material for various step rates. To

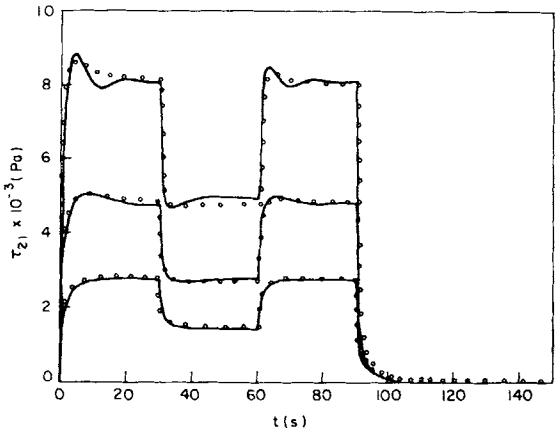

Figure 7 Comparison of (O) the measured shear stress with the predicted value of the NAN model. The rate and material parameters are the same as those in Figure 5. a = 0.92 for steps where $\dot{\gamma}$ = 0.5, and a = 0.93 for the other steps.

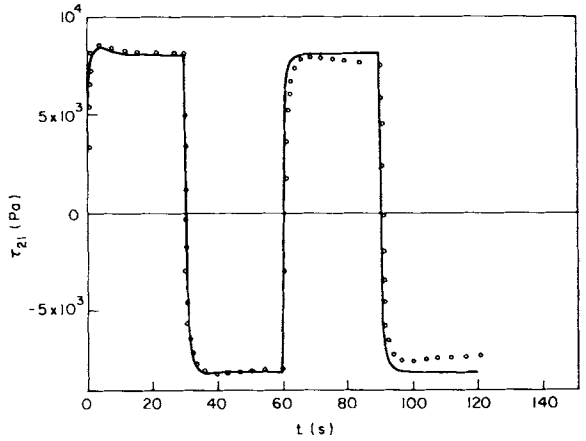

Figure 8 Shear stress for reversed shear steps. (—) Predictions of the RDN model. The model parameters are the same as those in Figure 5. (O) Data (PDMS).

achieve agreement between the predicted values and the experimental data, we multiply the moduli G_p [eq. (3d)] obtained from the linear regime by a constant (2.29). As can be seen from Figure 7, the agreement between the predictions and experimental measurements is reasonably good in both transient and steady situations. The predicted stress overshoot is greater than the measured one, especially at the highest shear rate. At high shear rates, the stress is predicted to oscillate and this is possibly due to the tumbling of the slipping structure that causes the major axis of the strain history to rotate.[11]

Reverse Shear

In a reverse shear flow, a constant shear rate is maintained for a length of time, and then the direction of the shear is reversed and kept at the same magnitude for another period of time. The fluid is sheared at a constant rate, but its direction alternates. The stress can be calculated from eq. (2a, b) for the RDN model. Figure 8 shows a comparison of the RDN model predictions with the experimental data of the PDMS melt. The agreement is equally good in the present flow. Similar agreement was obtained with the NAN model.

It has been shown that for the reverse shear flow, the Kaye-Bernstein–Kearsley–Zapas (K-BKZ) and the Doi–Edwards models poorly predict the stress.[11] One of the possible causes for this is that these models are strain dependent. It was pointed out that in flows where there is a jump discontinuity in shear rate, the stress might not depend only on the history of the strain.[12] A hybrid model in which strain and strain rate are involved explicitly might be superior to a purely strain or strain-rate model.

Large Amplitude Oscillation

In this flow, the strain varies sinusoidally with time and the amplitude of the oscillation is not small. It was found that if the strain amplitude is greater than 4, the free surface is distorted. The experimental data is limited to a strain amplitude of 4.

Giacomin and Oakley[13] compared the experimental results of the IUPAC LDPEX in large amplitude oscillations with the predictions of the models by Acierno et al., Moldenaers and Mewis, Mewis and De Cleyn, and Mewis and Denn. In their analysis they expressed the stress as a sum of odd harmonics, up to the third harmonic. The discrete Fourier transform is used to obtain each component.

In our case the stress is calculated from eq. (2a,b) and we obtained the stress from the start up of the flow. Figure 9 shows the calculated values of stress versus the shear strain and the shear rate for the RDN model. The values of the model parameters are the same as those considered in the previous two flows. We discretized the period into 24 and 48 steps. It can be seen from Figure 9 that, in the case of stress versus shear rate, the results using 24 and 48 steps are not markedly different. Due to nonlinearity and memory, the area of the stress against the shear rate loop is nonzero. The points in Figure 9 are joined linearly and so the curves are rather jagged. The convergence for the stress against shear is not as good as in the case of stress versus shear rate. We believe that 48 steps are adequate for the accuracy

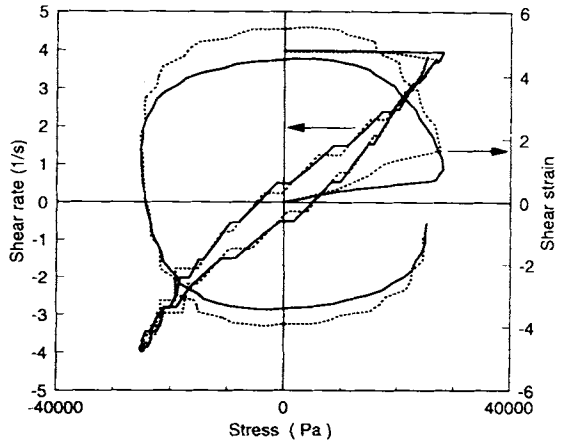

Figure 9 Stress (τ_{21}) versus strain (γ) and strain rate ($\dot{\gamma}$) for different steps. The frequency $\omega = 1$ rad/s, amplitude strain $\gamma = 4$, and model parameters are as in Figure 5. (—) 48 steps; (· · ·) 24 steps.

we can expect. In Figure 10 we compare the predicted values of the stress against the shear with the experimental values. The calculations are based on 48 steps. It can be seen that the agreement between the predictions and the measurement is good, including that at the start-up of the flow. We note that the predicted stress overshoot occurs earlier and is smaller in magnitude compared to the measured one.

Figure 11 shows the curves of stress versus strain and shear rate for shear amplitudes of 2 and 4. The curves are observed to be similar. The stress growth curves from the state of rest in both cases are identical.

CONCLUSIONS

A strain-rate dependence has been introduced in the integral constitutive equation of the finite linear viscoelasticity by

1. modifying the memory function so that it is both a function of time lapse and rate-of-strain; and
2. allowing the possibility of slippage and the Finger tensor is modified to a generalized strain.

Analytical expressions of the shear stress for arbitrary multi-rate-step flows for both models were derived. The predicted values of the shear stress agree reasonably well with the measured values of

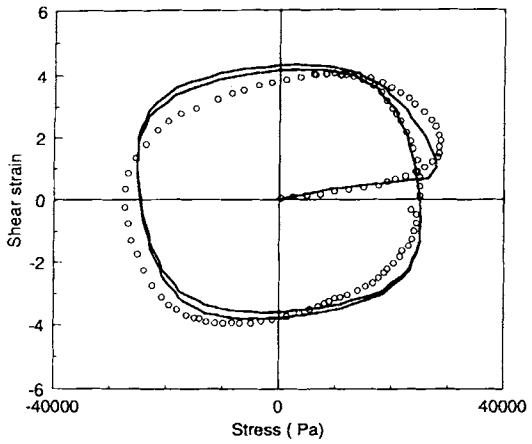

Figure 10 Stress (τ_{21})–strain (γ) evolution at large amplitude sinusoidal deformation amplitude strain and frequency as in Figure 9. The curve is the prediction of the RDN model using the model parameters given in Figure 5. (O) Data (PDMS).

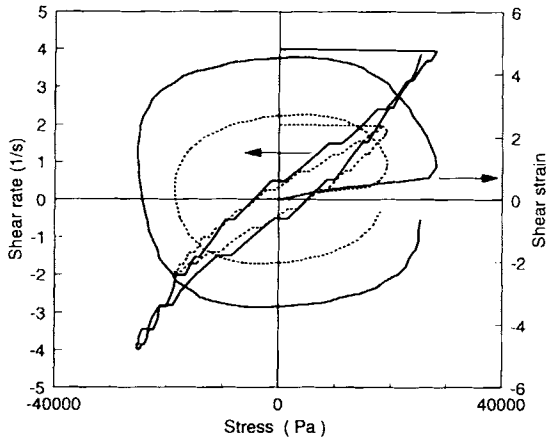

Figure 11 Stress (τ_{21}) versus strain (γ) and strain rate ($\dot{\gamma}$) for different amplitudes. The frequency model parameters are as in Figure 9 and the number of steps is 48. (—) amplitude 4; (· · ·) amplitude 2.

a PDMS melt in a concave flow, reverse flow, and large amplitude oscillatory flow. Appropriate values of G_p were introduced to successfully predict the shear stress in linear as well as nonlinear regimes. In a small amplitude oscillatory flow, the rate of change of entanglements is governed by the diffusion process only. In a finite deformation flow, both diffusion and deformation will contribute to the change of structure. Thus the data from dynamic tests only are insufficient.

We have shown that the constitutive equations considered in the present study are adequate for a PDMS melt in complex flows where a jump discontinuity in the shear rate is imposed. It is suggested that in flows where a jump discontinuity is imposed on the shear rate, a shear dependent constitutive equation might be inadequate.

It can be observed in Figures 5, 7, and 8 that the imposed step jumps in the shear rate lead to step jumps in the shear stress. In step-strain experiments, the shear stress usually undergoes a more gradual change.[3,11] It may be desirable to test the present constitutive equations for step-strain data. However, it can be argued that the step-strain rate experiment is a more severe test to evaluate constitutive equations. In addition, equations that adequately describe step-strain rate experiments can describe step-strain experiments equally well. This is confirmed for the large amplitude oscillatory flow where the strain is changed sinusoidally and the stress versus the strain curves are smooth, as shown in Figures 9–11.

D. De Kee wishes to acknowledge financial support from the Natural Sciences and Engineering Research Council

of Canada. Also, the award of an NSERC International Scientific Exchange Award made Y. Xu's participation possible. The authors thank the Rheometrics Co. for the measurements of the experimental data.

REFERENCES

1. J. M. Dealy and K. F. Wissbrun, *Melt Rheology and Its Role in Plastic Processing. Theory and Applications,* Van Nostrand Reinhold, New York, 1990.
2. K. Osaki and M. Kurata, *Macromolecules,* **13,** 671 (1980).
3. K. Osaki, S. Kimura, and M. Kurata, *J. Rheol.,* **25,** 549 (1981).
4. C. M. Vrentas and W. W. Graessley, *J. Rheol.,* **26,** 359 (1982).
5. J. S. Vrentas, C. M. Vrentas, and D. C. Venerus, *Macromolecules,* **23,** 5133 (1990).
6. D. C. Venerus and H. Kahvand, *J. Rheol.,* **38,** 1297 (1994).
7. Y. Z. Xu, D. De Kee, and C. F. Chan Man Fong, *J. Appl. Polymer Sci.,* **55,** 779 (1995).
8. D. De Kee, Ph.D. thesis, University of Montreal, 1977.
9. J. D. Ferry, *Viscoelastic Properties of Polymers,* 2nd. ed., Wiley, New York, 1970.
10. N. W. Tschoegl, *The Theory of Linear Viscoelastic Behavior,* Springer–Verlag, New York, 1988.
11. R. G. Larson, *Constitutive Equations for Polymer Melts and Solutions,* Butterworths, New York, 1988.
12. J. G. Oldroyd, *Proc. Roy. Soc.,* **A283,** 115 (1965).
13. A. J. Giacomin and J. G. Oakley, *J. Rheol.,* **36,** 1529 (1992).

Received April 12, 1995
Accepted July 26, 1995